

Supercharging Imbalanced Data Learning With Causal Representation Transfer

Junya Chen*, Zidi Xiu*, Benjamin Goldstein, Ricardo Henao, Lawrence Carin, Chenyang Tao

{junya.chen, zidi.xiu, ben.goldstein, ricardo.henao, lcarin, chenyang.tao}@duke.edu

Abstract

Dealing with severe class imbalance poses a major challenge for real-world applications, especially when the accurate classification and generalization of minority classes is of primary interest. In computer vision, learning from long tailed datasets is a recurring theme, especially for natural image datasets. While existing solutions mostly appeal to sampling or weighting adjustments to alleviate the pathological imbalance, or imposing inductive bias to prioritize non-spurious associations, we take novel perspectives to promote sample efficiency and model generalization based on the invariance principles of causality. Our proposal posits a meta-distributional scenario, where the data generating mechanism is invariant across the label-conditional feature distributions. Such causal assumption enables efficient knowledge transfer from the dominant classes to their under-represented counterparts, even if the respective feature distributions show apparent disparities. This allows us to leverage a causal data inflation procedure to enlarge the representation of minority classes. Our development is orthogonal to the existing extreme classification techniques thus can be seamlessly integrated. The utility of our proposal is validated with an extensive set of synthetic and real-world computer vision tasks against SOTA solutions.

1. Introduction

Learning with imbalanced datasets is a norm in modern computer vision, and more generally in many other machine learning applications, with great challenges entailed. Typical scenarios include: (i) rare events, where the event prevalence is extremely low while their consequence is of high cost (e.g., severe risks that people seek to avert [36]); (ii) emerging objects in a dynamic environment, calling for quick adaptation of an agent to identify new cases with only a handful target examples and plentiful past experience [22]. In the vision domain, a more characteristic scenario is that the natural occurrence of different visual objects typically follows a power law distribution, and the

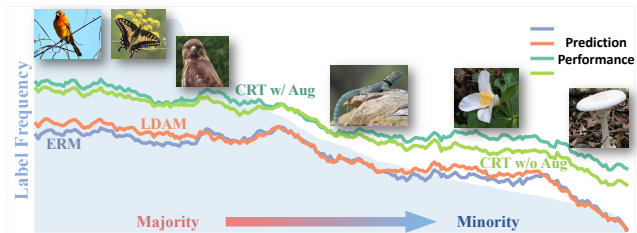


Figure 1. Causal representation transfer alleviates tail imbalance.

accurate identification of those rarer instances bears significant social-economic values (e.g., fraud detection [17], driving safety [19], nature conservation [33], social fairness [11] and public health [42]).

Notably, severe class imbalance and lack of minority labels are the two major difficulties prompted in this setting, which render standard learning strategies unsuitable [37]. Without explicit statistical adjustments, the imbalance induces bias towards the majority classes; on the other hand, the lack of minority representations prevents the identification of non-spurious associations that generalize. The growing capacity of data collection procedures also inadvertently exacerbates the issue, via feeding an excess of predictors relative to the limited occurrence of events.

Various research efforts have been directed to ameliorate the above issues, with re-establishing the balance as the most popular heuristic. The two most prominent directions in the category include statistical resampling and reweighting. Resampling alters the exposure frequency during training, i.e., more for the minorities and less so for the majorities [20]; and reweighting instead, directly amends the relative importance of each sample based on their class [16], sampling frequency [4] and associated cost for misclassification [21]. Recent developments also considered class-sensitive and data-adaptive losses to more flexibly offset the imbalance [7, 40]. While being intuitive and works reasonably well in practice, an important caveat with these proposals is that they offer no protection against the overfitting of minority instances, a fundamental obstacle towards better generalization.

To get around this limitation, one promising thought is to solicit inductive bias, imposing strong constraints to sup-

*contributed equally to this work.

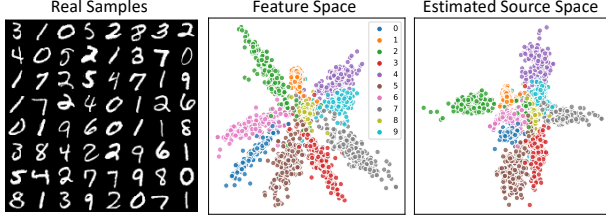


Figure 2. Comparison of data space \mathcal{X} , feature space \mathcal{Z} (predictive but entangled) and CRT identified source space \mathcal{S} (independent/disentangled) representations for the MNIST digits.

press spurious fits that hinder out-of-sample predictions. A classical setup is few-shot learning [63], where the majority examples are used to train meta-predictors and transferable features, leaving only a few parameters to tune for the minority data. In anomaly detection, methods such as one-class classification instead postulate minority are outliers that do not always associate with stable, recognizable patterns [45, 53]. While capitalizing on their superior ability in generalizing in the low sample regime, these approaches operate under fairly strong assumptions and inadequately account for the information from the minorities.

More recently, establishing causal invariance emerged as a new, powerful learning principle to approach better generalization even under apparent distribution shifts [51]. In contrast to standard empirical risk minimization schemes, where the generalization to similar scenarios is considered, causally-inspired learning instead embraces robustness against potential perturbations [2]. This is achieved via only attending to causally relevant features and associations postulated to be invariant under different settings [48]. In other words, contributions from spurious, unstable features are effectively blocked or attenuated. Interestingly, compromise of utility can be expected in those models [52], as a direct consequence for ditching useful (but non-causal) correlations to trade for better causal generalization.

This study is an exploration of advancing imbalanced data learning via infusing causal perspectives. In recognition of the limitations discussed above, we present *causal representation transfer* (CRT), a novel imbalanced learning scheme that brings together ideas from causality, contrastive learning, data-augmentation and weakly-supervised learning, to address the identified weakness of existing solutions. Our key contributions include: (i) a causal representation encoder informed by an invariant generative mechanism based on generalized contrastive learning; (ii) a data-augmentation procedure exploiting feature independence to enrich minority representations; (iii) regularized source representation modeling techniques that better balance the trade-off between utility and invariance; (iv) new theoretical views explaining why our proposal works. Notably, our development is complementary to existing models and can be easily integrated to promise further synergies.

2. Preliminaries

Notations and problem setup. We use $\mathbf{x} \in \mathbb{R}^p$ to denote the original input data and $\mathbf{z} \in \mathbb{R}^d$ for the predictive features extracted. Let $y \in [M]$ be the class label and use $m \in [M]$ to index the m -th class. The number of total training samples and those with label m are respectively denoted as n and n_m . We use \mathbb{E}_i to denote the average of an empirical distribution, \mathbf{a}_i to denote a vector associated with the i -th sample, and $[\mathbf{a}]_b$ to denote the b -th dimension of a vector \mathbf{a} . To keep our discussions simple, we always assume class M is the minority class, i.e., $n_m \gg n_M, \forall m \in [M-1]$. Throughout this paper, we refer to \mathcal{X} , \mathcal{Z} and \mathcal{S} respectively as data, feature, and source space (see Figure 2), with their definitions to be clarified later. Our goal is to accurately predict the label of minority instances with very limited training examples from the same class. Generalization to multiple minority categories is straightforward.

2.1. Generalized contrastive learning and ICA

Independent component analysis (ICA), also known as *blind source separation* (BSS) in some contexts, seeks to address the inverse problem of signal disentanglement [29]. More specifically, ICA de-correlates the observed signal \mathbf{Z} to a source signal representation $\mathbf{S} = f(\mathbf{Z})$, where $f(\mathbf{z})$ is a smooth, invertible mapping known as the *de-mixing* function, such that the components of source \mathbf{S} are assumed to be statistically independent (i.e., $p(\mathbf{s}) = \prod_j p_j([s]_j)$). For convenience, we call such $p_j([s]_j)$ *independent component distributions* (IC distributions). While one can recover $f(\mathbf{z})$ assuming the non-Gaussianity of \mathbf{S} in the linear case (i.e., $f(\mathbf{z})$ is linear [13]), it is in general infeasible for arbitrary nonlinear $f(\mathbf{z})$ without further assumptions [30]. Recently, [31] proposed a setting where the identification of *nonlinear ICA* (NICA) can be achieved (Figure 3), which requires an additional auxiliary variables \mathbf{c} . Informally, it makes the assertion that assuming the source signals are conditionally independent given the auxiliary \mathbf{c} (i.e., $p(\mathbf{s}|\mathbf{c}) = \prod_j p_j([s]_j|\mathbf{c})$), then $f(\mathbf{z})$ can be identified via a technique known as the *generalized contrastive learning* (GCL).

Implementation-wise, GCL solves for a simple Logistic regression problem. Let $r_\gamma(\mathbf{z}, \mathbf{c}) = \sum_{a=1}^d \gamma_a([\hat{\mathbf{s}}]_a, \mathbf{c})$ be the critic function, where $\hat{\mathbf{s}} = f_\psi(\mathbf{z})$. Then GCL optimizes for the following contrastive learning objective

$$\arg \min_{\mathbf{f}_\psi, r_\gamma} \underbrace{\{\mathbb{E}_i[\phi(-r(\mathbf{z}_i, \mathbf{c}_i))] + \mathbb{E}_{j \neq i}[\phi(r(\mathbf{z}_i, \mathbf{c}_j))]\}}_{\mathcal{L}_{\text{GCL}}(\mathbf{f}_\psi, r_\gamma)}, \quad (1)$$

where $\phi(r) = \log(1 + \exp(r))$ denotes the Softplus function. Note (1) is a Logistic regression that contrasts congruent pairs $(\mathbf{z}_i, \mathbf{c}_i)$ against incongruent pairs $(\mathbf{z}_i, \mathbf{c}_j), i \neq j$ to maximize the discriminative power, which leads to the identification of $f(\mathbf{z})$. We refer readers to our

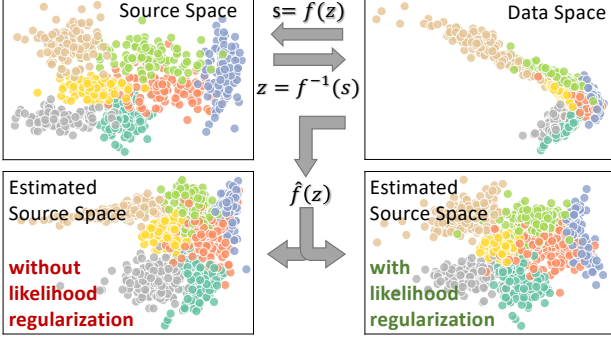


Figure 3. Despite apparent disparities in distribution, a common causal generative mechanism is shared across different groups.

supplementary material (SM) for a more formal technical exposition.

2.2. Invertible neural network

The recent surge of interest in generative modeling popularizes the use of *invertible neural networks* (INN) in machine learning, with prominent examples such as normalizing flows [49] and neural ODEs [9]. Unlike standard neural networks, INN seeks to establish a one-to-one mapping between the input and output domains (*i.e.*, the forward map $s = f(z)$ and the associated reverse map $z = f^{-1}(s)$). The standard construction is to consider stacking simple invertible transformations to build up flexible invertible neural nets. Practical trade-offs are often considered between the ease of forward and inverse passes depending on applications [47]. In this work, we desire fast forward computations, and adopt the *masked auto-regressive flow* (MAF) design for our invertible neural net [47], which is an implementation of scale-and-shift transforms that employs causal masking to enable parallel computation of an auto-regressive architecture.

More specifically, let $\{z^t\}_{t=0}^T$ be a length- T flow, which means $z^0 = z, s = z^T$. Then MAF is defined by $z^{t+1} = a_t \odot z^t + b_t$, where a_t, b_t are functions of z^t , respectively known as the scale and shift terms, subject to the constraint that the i -th output in a_t, b_t only depends on $[z^t]_{<i}$, *i.e.*, conforming to the causal structure of an auto-regressive flow. Shuffling layers are inserted to avoid order-dependent degeneracies. Many applications of INN, generative flows in particular, also seek a tractable Jacobian $J(z) \triangleq |\det(\nabla_z f)|$ of $f(z)$ to enable likelihood computations. Assuming the source representation S has density $p_0(s)$, the data likelihood $p(z)$ of a scale-and-shift flow model is given by

$$\begin{aligned} \log p(z) &= \log |\det(\nabla_z f_\psi)| + \log p_0(s) \\ &= \sum_t \log |a_t(z^t)| + \log p_0(s) \\ &\triangleq \mathcal{L}_{\text{FLOW}}(z; f_\psi) \end{aligned} \quad (2)$$

Algorithm 1 Causal Representation Transfer

1. Pretrain encoder and predictor
 $e_\theta, h_{\phi'} \leftarrow \arg \min \{\mathbb{E}_i[\ell(h(e(x_i)), y_i)]\}$
2. NICA estimation with $z = e_\theta(x)$
 $f_\psi \leftarrow \text{GCL}(\{(z_i, c_i)\})$
3. Source space augmentation with $s = f_\psi(z)$
 $(\tilde{s}, c), [\tilde{s}]_j = [s_{k_j}]_j, \text{ s.t. } k_j \stackrel{\text{unif}}{\sim} \{i : c_i = c\}$
4. Predictor modeling with augmented source
 $h_\phi \leftarrow \arg \min \{\mathbb{E}_i[\ell(h(s_i), y_i)] + \lambda \mathbb{E}[\ell(h(\tilde{s}), \tilde{y})]\}$

3. Causal Representation Transfer

In this section, we detail our construction of *causal representation transfer* (CRT), a novel causally informed data transformation & augmentation procedure to empower the learning of imbalanced datasets. Our model posits a shared data-generation procedure (*i.e.*, the underlying causality), which can be accurately identified by learning with the majority classes, assuming class-conditional representation independence. Through the inversion of this data generation mechanism, we obtain de-correlated, permutation-invariant representations of the data, to be exploited for efficient learning and augmentation.

Our model is comprised of the following components: (i) a feature encoder module $z = e_\theta(x)$; (ii) two classification modules $h_{\phi'}(z), h_\phi(s)$ for prediction; (iii) a nonlinear ICA module for representation de-mixing $s = f_\psi(z)$; (iv) an auxiliary critic module $r_\gamma(f_\psi(z), c)$ for GCL; and (v) a data inflation module. Algorithm 1 outlines a general working flow, and in the following sections we will elaborate our assumptions and detail the implementation of CRT.

3.1. Model assumptions

To enable knowledge transfer between classes, we make the following assumptions:

Assumption 3.1. Let z be the sufficient statistics (features) of x for predicting label y , and all class conditional feature distributions $p(z|y)$ share a common ICA de-mixing function $f(z)$.

In other words, there exists a smooth invertible function $f : \mathbb{R}^d \rightarrow \mathbb{R}^d$, and a set of IC distributions $q_m(s)$, that link to the predictive feature distributions $p_y(z)$ via $S^y = f(Z^y)$, where $S^y \sim q_y(s)$ and $Z^y \sim p_y(z)$, where we used $p_y(z)$ for $p(z|y)$. We consider $f^{-1}(s) : S \rightarrow \mathcal{Z}$ as the invariant causal mechanism underlying our data, see Figure 3 for a graphical illustration. These conditions enable the identification of the shared commonality, namely the de-mixing function $f(z)$, that formally relates the possibly very dissimilar distributions $p_y(z)$.

A valid criticism is that Assumption 3.1 seems very strong, and is unlikely to hold realistically. We argue that in practice these conditions should be considered as structural

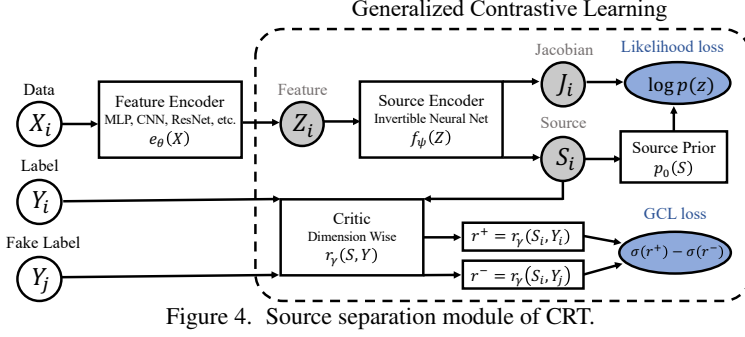


Figure 4. Source separation module of CRT.

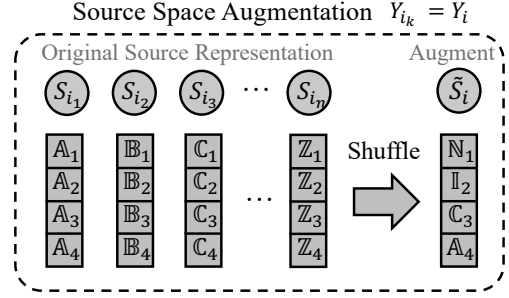


Figure 5. Source augmentation.

constraints to restrict the search space of a solution. In other words, we are imposing causal constraints to find a more effective knowledge transfer mechanism. This encourages the exploitation of shared commonalities in data, and the solutions should be interpreted in an approximate sense: a model with the least violation of assumed causal constraints would be expected to maximally empower transferability.

3.2. Causal Representation Transfer

Encoder pre-training. To implement CRT, our first step is to find a good reduced feature representation of \mathbf{x} highly predictive of label y . This can be simply achieved by the supervised representation learning (see Figure 4, Figure 6), optimizing an encoder and predictor pair $(e_\theta(\mathbf{x}), h_{\phi'}(\mathbf{z}))$ to minimize the label prediction risk $\mathcal{L} \triangleq \mathbb{E}[\ell(h_{\phi'}(e_\theta(\mathbf{x})), y)]$ (e.g., cross-entropy, hinge loss, etc.). To avoid capturing spurious features that overfits minority data, one could train with majority samples only in this stage, to learn more stable representations. Alternatively, one could also consider unsupervised feature extraction schemes, such as auto-encoders. The employment of statistical adjustments, such as importance weighting, can be considered to reduce the impact of data imbalance.

De-mixing representation with GCL. After obtaining a good feature representation $\mathbf{Z} = e_\theta(\mathbf{X})$, our next step is to learn a de-mixing function $\mathbf{f}_\psi(\mathbf{z})$, such that the source representation $\mathbf{S} = \mathbf{f}_\psi(\mathbf{Z})$ is approximately independent given the class label. This can be easily done by optimizing the GCL objective (1) wrt feature representation and label pairings $\{(\mathbf{z}_i, y_i)\}$, using MAF to model the smooth, invertible transformation $\mathbf{f}_\psi(\mathbf{z})$. Similarly, this stage also does not necessarily need to involve the minority data. See Figure 4 for a graphical illustration.

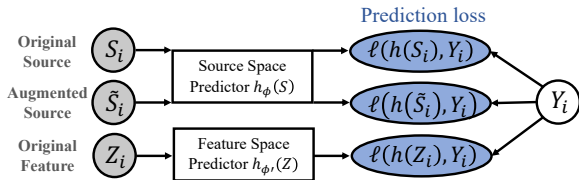


Figure 6. Prediction modules.

Augmenting the minority. Inspired by [58], we artificially enrich minority representations via data shuffling in the source space (see Figure 5). Under the assumed conditional independence, feature vector \mathbf{Z} corresponding to label y is generated by $\mathbf{Z} = \mathbf{f}^{-1}(\mathbf{S})$, where $[\mathbf{S}]_j \sim q_j(s|y)$ are independently sampled. This implies if we are able to sample from each marginal distributions given y , then we can synthesize new samples for \mathbf{Z}_y . Using the estimated de-mixing function \mathbf{f}_ψ , we are able to obtain an approximate empirical source distribution for each corresponding y : $\mathbf{S}^y \triangleq \{\mathbf{s}_i = \mathbf{f}(e_\theta(\mathbf{x}_i)) | y_i = y\} = \{\mathbf{s}_k^y\}_{k=1}^{n_y}$, assuming n_y units in \mathbf{S}^y reindexed by k . Then drawing new samples $\tilde{\mathbf{s}}^y$ from the empirical $\hat{p}(\mathbf{s}|y)$ amounts to shuffling the index k for each dimension independently, i.e.,

$$\tilde{\mathbf{s}}_k^y = ([\mathbf{s}_{k_1}^y]_1, [\mathbf{s}_{k_2}^y]_2, \dots, [\mathbf{s}_{k_d}^y]_d), \quad (3)$$

where $\mathbf{k} = (k_1, \dots, k_d) \in [n_y]^d$, and we call this *non-parametric augmentation*. Inverting $\tilde{\mathbf{s}}^y$ with the estimated \mathbf{f}_ψ synthesizes a feature vector $\tilde{\mathbf{z}}^y = \mathbf{f}_\psi^{-1}(\tilde{\mathbf{s}}^y)$ for label y . In our next section, we will argue this inversion is not only costly but also suboptimal, and should be avoided.

Model refinement. Now we may leverage the augmented data to refine our prediction model. For minority class $y = M$, we optimize the following objective

$$\mathcal{L}_{\text{aug}}(\phi') = \mathcal{L}(\phi') + \lambda(\mathbb{E}_{\mathbf{Z}^M}[\ell(h_{\phi'}(\tilde{\mathbf{Z}}^M), M)] - \mathbb{E}_{y_i=M}[\ell(h_{\phi'}(\mathbf{z}_i), M)]), \quad (4)$$

where $\lambda \in [0, 1]$ is a factor that encodes the relative confidence for trusting the artificially inflated representations $\tilde{\mathbf{Z}}^M$ for minority label $y = M$. Here we have fixed the encoder module, since changes to the encoder will propagate to the de-mixing function, thereby destabilizing training via compromising the validity of the augmented samples.

Challenges with naïve implementation. We identify three major issues with the naïve implementation of CRT, to be addressed in the section below.

- **Representation collapse.** GCL solution is not unique, suboptimal ones degrade stability & performance.
- **Costly augmentation.** MAF inversions dominate the computation burden during training.
- **Gridding artifact.** Small minority sample size leads to pronounced augmentation bias (see Figure 7).

3.3. Improving causal representation transfer

Regularizing the data likelihood. The theory of NICA only asserts that in the asymptotic limit, the source representation will be identified up to an invertible transformation of each dimension. This leaves room for further improvement: there might be a myriad of valid source representations, and while all feasible representations are equal in the eyes of ICA, their predictive performance can vary significantly. This intuition is readily confirmed via empirical observation: naïve implementation of NICA often yields pathological representations that where data points are compressed into narrow stripes, even thin lines in the source space (see Figure 3). To decode back to the feature space and make useful predictions, the neural network will need to be expansive (*i.e.*, requiring a large Lipschitz constant), thereby sacrificing network stability and model generalization according to standard learning theories [14, 61]. Intuitively, if samples are very close to each other in the representation space, it will be more difficult for a learning agent to accurately & robustly map the decision boundaries.

To encourage more spread-out representations, we consider a simple, intuitive fix, that is to regularize source representation with the data log-likelihood (in feature space). This amounts to the simple summation of the log of scale terms and the source likelihood (*c.f.*, ℓ_{FLOW} defined in (2)). Following popular practice, we set source measure $p_0(s)$ to the standard Gaussian, and optimize the following likelihood-regularized GCL objective

$$\tilde{\mathcal{L}}_{\text{GCL}}(\mathbf{f}_\psi, r_\gamma) = \mathcal{L}_{\text{GCL}}(\mathbf{f}_\psi, r_\gamma) + \lambda \mathcal{L}_{\text{FLOW}}(\mathbf{f}_\psi), \quad (5)$$

where $\lambda > 0$ is the regularization strength. This will push the global source representation identified by GCL towards a Gaussian-like shape.

Note that we can interpret the likelihood-regularized objective (5) as a relaxation to the conditional independence assumption 3.1. To see this, recall the likelihood objective (2) tries to map the source representations to be *unconditionally* independent, as oppose to the *conditional* independence assumed by NICA. It provides a “*fall-back*” mode in case Assumption 3.1 is violated to some extent. This also motivates us to consider an important variant: making class-dependent source measures, *i.e.*, $p_0^c(s)$ for each class label c . Compared to the fully non-parametric objective (1), this strategy further encourages the source representations to be independent given the class labels, and it allows parametric data augmentation (*i.e.*, sampling from the parametric label priors instead of permuting the indices). To enable extra flexibility, one may consider modeling each marginal distribution $p_0^c([z]_j)$ with Gaussian mixtures.

Modeling in the source space. Rather than modeling the predictor $h_{\phi'}(z)$ in the feature space \mathcal{Z} , we advocate instead building the predictor directly in the source space \mathcal{S} , *i.e.*, modeling with $h_\phi(s)$. This practice enjoys several

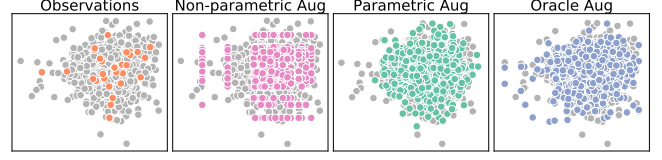


Figure 7. Comparisons of different source augmentations overlaid on the ground-truth distribution (gray). Severe gridding artifact in the low-sample regime for the nonparametric scheme.

benefits: (i) *Easy & robust augmentation*: many designs of high-dimensional flows are asymmetric computationally, and inverting a MAF is not only d times more costly than a forward pass, it is also unstable at the boundary points. Direct modeling in the source space bypasses the costly and unstable MAF inversions to synthesize feature representations for data augmentation; (ii) *Feature whitening*: normalization has long been considered as an integral part of data analysis, supported by abundant empirical evidence. CRT features a representation that component-wise independent, and consequently interchangeable within class.

Parametric augmentation. When the number of minority observations is small, the indices shuffling based non-parametric augmentation procedure described above will suffer from the *gridding artifact* (See Figure 7), resulting from the lack of representation diversity. This artifact can be detrimental, amplifying the augmentation bias in the low sample regime. To overcome this limitation, we empirically observe that the empirical estimate of class-conditional source distributions are usually Gaussian like after the likelihood regularization, and especially so when the label conditional prior is adopted. In these situations, parametric augmentations, where one samples synthetic source samples from a Gaussian distribution characterized by the empirical mean and variance of minority source representations, are statistically more efficient.

3.4. Theoretical insights and remarks

Why causal augmentation works. It is helpful to understand the gains from CRT’s causal augmentation beyond the heuristic that shuffling the ICs provides more training samples for the minority class. [58] considered a similar causal augmentation procedure for few-shot learning, and provided two major theoretical arguments: (i) the risk estimator based on the augmented examples is the uniformly minimum variance unbiased estimator given. accurate estimation of \mathbf{f}_ψ (Theorem 1, [58]) ; (ii) with high probability the generalization gap can be bounded by the approximation error of \mathbf{f}_ψ (Theorem 2, [58]) .

To complement the above augmentation-based reasonings, here we provide alternative views, to further justify our GCL-based causal representation disentanglement. We only present informal, heuristic arguments in the main text, with more rigorous statements deferred to our SM. Our

claims will be verified in the Experiment section.

Speedup from weakly-supervised learning. While for typical supervised learning tasks the generalization bound scale as $\mathcal{O}(n^{-\frac{1}{2}})$, [50] showed that, a superior rate of $\mathcal{O}(n^{-\eta})$, where $\eta \in [\frac{1}{2}, 1]$ is possible (Theorem 3, [50]), provided there exists abundant data for an alternative, yet related *weak* task. Note n refers to the size of labeled data directly related to the *strong* task of interest (in our case, prediction of minority labels). The general sufficient condition for that improved rate to be feasible is the existence of a shared mutual embedding for both the weak and strong tasks [50]. CRT leverages GCL as the weak task to help learn the shared source space embedding using the majority examples, thereby improving the prediction of minorities.

Representation whitening and disentanglement. Our CRT executes a special kind of representation disentanglement [56, 59] that conforms to a causal rule, via de-correlating the representations conditionally. Extensive empirical evidence has pointed to the fact that such representation de-correlation, more commonly known as data whitening [34], is expected to improve learning efficiency [12]. Theoretically, this may result from the improved conditioning of Fisher matrix for gradient-based optimization [18], which motivates the development of specialized network architectures that promote a de-correlated data representation internally [28, 3, 32]. Our source space modeling explicitly separates the task of representation disentanglement, in turn helps the prediction network to focus on its primary goal.

Potential limitations. We caution there is more nuisance involved in the discussion. The setting considered by CRT is restrictive in the sense that it precludes the learning of useful, yet **non-transferable** features predictive of the minority labels. For instance, there might be a unique, possibly deterministic signature u for the minority class. However, since the de-mixer is only trained on the majority domains absent of this signature, there is no way this feature can be exploited by our CRT model. This points to a key limitation of causally inspired models, that they are often too conservative for only retaining the invariant features, promoting cross-domain generalizability at the price of within-domain predictive performance degradations [52]. Formulating a hybrid solution that combines the wisdom of other imbalanced learning strategies promises to overcome this limitation, and we leave it for future investigations.

4. Related Work

Causal invariance and representation learning. A major school of considerations for building robust machine learning models is to stipulate invariant causal relations across environments [54], such that one hopes to safely extrapolate beyond the training scenario [5]. We broadly categorize such efforts into two streams, namely predictive causal models and generative causal models. Prominent exam-

ples from the first category include ICP [48, 27] and IRM [2], highlighting the identification of invariant representation and causal relations via penalizing environmental heterogeneities. Our solution pertains to the second category, where the data distribution shifts across environments can be tethered by an invariant generation procedure [31, 35]. This work exploits the recovered causally invariant source representation to mitigate the sample scarcity of minority labels in imbalanced sets.

Learning with imbalanced data. Resolving data imbalance is a heavily investigated topic to overcome the curse of long-tail distributions [41]. The standard practice of sampling and weight adjustment have been proved useful, although with their own caveats in information loss and introducing bias. Due to these concerns, recent literature has actively explored adaptive strategies, such as redundancy-adjusted effective sample size to construct better balancing weights [16], and the use of the theoretically grounded class-dependent margins adapted to the sample size [7]. In a similar vein to *boosting* [24], adaptive weights are proposed to prioritize the learning of less well-classified examples [40] while excluding apparent outliers [38]. Much related to our setting are the *meta-learning* scenarios [62, 23, 64], where a learning agent tries to generalize & repurpose the knowledge learned from majority classes to minority predictions; and also the augmentation-based schemes to restore class balance [43, 46].

Data augmentation. Due to its exceptional effectiveness, augmentation schemes are widely adopted in machine learning applications [55]. Most popular augmentation strategies are built on known invariant transformations (e.g., rotation, scaling, noise corruption, etc.) [57], simple interpolation heuristics [8, 26], and more recently towards fully auto-mated procedures [15]. Notably, a recent trend extended the focus of data augmentation to robust learning against adversarially crafted inputs [25]. The progress in distribution learning also inspires generative augmentation procedures that compose realistic artificial samples [1].

Domain adaption and causal mechanism transfer. Closest to our contribution is the work of *causal mechanism transfer* (CMT) [58], which focused on addressing the challenge of few-shot learning for continuous regression. There are a few major differences that distinguish our work from this predecessor: CMT focused on domain adaptation and does not address classification; it bundles (x, y) for NICA which necessitates the flow inversion for sample augmentation. Grounded in the setting of imbalanced data learning, our CRT extends applications and advocates source space modeling to simplify & improve the causal augmentation. It also features likelihood regularization to enhance representation regularity. Alternative theoretical insights have been discussed to justify the use of NICA-based augmentation, complementing the analysis from the CMT paper.

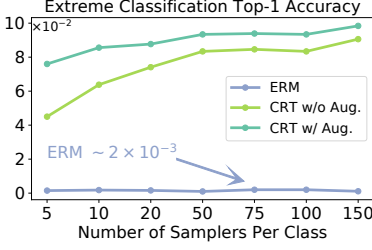


Figure 8. Extreme classification of 1k labels. ERM performs slightly better than random guess, while CRT works significantly better.

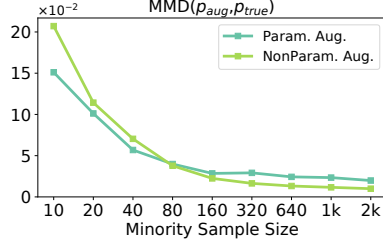


Figure 9. Comparison of different causal augmentations. (lower is better) Parametric augmentation is more efficient with small samples.

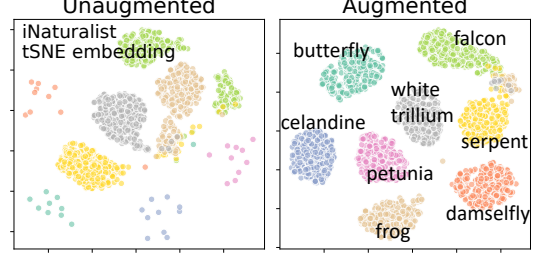


Figure 10. CRT source representation trained on iNaturalist, visualized using tSNE embedding in two dimensions for eight random categories.

5. Experiment

To validate the utility of our model, we consider a wide range of (semi)-synthetic and real-world tasks experimentally. All experiments are implemented with PyTorch, and our code is available from <https://github.com/ZidiXiu/CRT>. Limited by space, more detail of our setups & additional analyses are deferred to the SM.

5.1. Experimental setups

Baselines. The following set of competing baselines are considered to benchmark the proposed solution: (i) Empirical risk minimization (ERM), naïve baseline with no adjustment; (ii) Importance-weighting (IW) [6], a class-weight balanced training loss; (iii) Generative adversarial augmentation (GAN) [1], synthetic augmentations from adversarially-trained sampler; (iv) Virtual adversarial training (VAT) [44], robustness regularization with virtual perturbations; (v) FOCAL loss [40], cost-sensitive adaptive weighting; (vi) Label-distribution-aware margin loss (LDAM) [7], margin-optimal class weights.

Evaluation metrics & setup. To quantitatively assessing the performance of competing models, we consider the following performance measures for the classification tasks: (i) *negative log-likelihood* (NLL), also known as *cross-entropy*; (ii) minority F1 score; (iii) *Top-k* accuracy ($k = 1, 5$). We adopt the classical evaluation setup for imbalanced data learning, which learns on an imbalanced training set and reports performance on a balanced validation set.

Model architecture, hyper-parameter and data-preprocessing. In our implementations, for large image models (*i.e.*, iNaturalist, TinyImageNet) we apply pre-trained CNN to extract vectorized image representations as raw inputs, which is subsequently fed into a fully-connected multi-layer perceptrons (MLP) for feature encoding. For small image models (*i.e.*, MNIST, CIFAR100) we directly train a CNN from scratch for feature extraction. We used a random 8/2 split for training and validation purposes, and applied Adam optimizers to learn model parameters. We rely on the best out-of-sample cross-entropy and GCL loss for model selection and hyper-parameter tuning.

5.2. Synthetic data and ablation study

Toy model. Toy data from the following models summarizes challenges from real-world data: first sample from m uncorrelated 2D Gaussians with different means and variances as source representation s , each assigned to a different label. s is then distorted into \tilde{s} by applying a few rotations and scaling, followed by the classical Hénon transformation $z_1 = 1 - 1.4\tilde{s}_1^2 + \tilde{s}_2, z_2 = 0.3\tilde{s}_1$, to induce more complex association structures. Finally we apply a random affine transformation and corrupt the data with random Gaussian noise, *i.e.*, $x = Az + \epsilon$, ($A \in \mathbb{R}^{32 \times 2}, \epsilon \in \mathbb{R}^{32}$ iid standard Gaussian). See our SM for detailed specifications.

Figure 3 compares GCL-based NICA with and without likelihood penalty, where the estimated source representations appear more spread-out with regularization. To quantitatively compare the augmentation efficiency, in Figure 9 we compare the MMD distance between the different augmentation outputs and the ground-truth, confirming the improved efficiency from the CRT parametric augmentation in the low-sample regime.

Extreme classification. Related to the challenge of imbalanced data learning is the extreme classification [10], where the label size is huge but there is only a handful of samples pertaining to each label class. In Figure 8, we show the proposed CRT fares very well in this scenario, while standard ERM struggles. This result also indicates that with the abundance of different class labels, GCL is robust to overfitting even if the per-class sample size is small.

5.3. Evaluation on real-world vision datasets

Datasets. To benchmark CRT against its SOTA alternatives in realistic settings, we consider the following semi-synthetic and real datasets: (i) *Imbalanced MNIST and CIFAR100*: we create imbalanced versions of these standard image classification tasks, following [7], two types of imbalance are of interest: long-tailed imbalance (exponential decay in class-sample size) and step imbalance (fixed imbalance ratio between majority and minority); (ii) *Imbalanced TinyImageNet* [65]: a scaled-down version of the classic natural image dataset ImageNet, comprised of 200

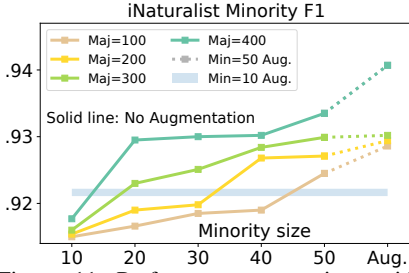


Figure 11. Performance comparison with and without augmentations. Augmented solutions boosts effective sample size.

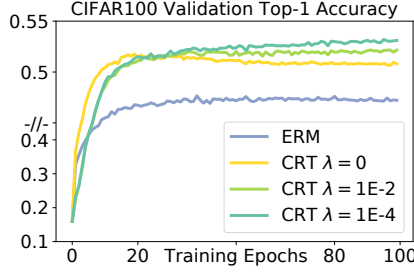


Figure 12. Comparison of learning dynamics. CRT enables both faster learning and better model predictions.

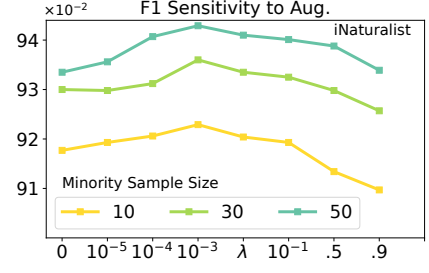


Figure 13. Sensitivity analysis of augmentation strength λ . A smaller minority sample size is more sensitive to the augmentation.

Table 1. Comparison of performance on real-world datasets

	CIFAR100			iNATURALIST			TINYIMAGENET		
	TOP-1 \uparrow	TOP-5 \uparrow	NLL \downarrow	TOP-1 \uparrow	TOP-5 \uparrow	NLL \downarrow	TOP-1 \uparrow	TOP-5 \uparrow	NLL \downarrow
ERM	49.29	78.22	2.95	66.73	87.86	1.70	58.52	79.01	3.22
IW	43.97	68.96	3.89	67.63	88.94	1.66	60.50	80.23	2.92
GAN	47.64	78.53	2.69	67.40	87.00	1.82	60.69	80.91	2.33
VAT	46.47	74.23	3.19	67.06	87.39	1.90	59.69	82.05	2.42
FOCAL	43.32	74.39	2.89	66.63	88.45	1.59	58.27	79.39	2.59
LDAM	50.46	74.39	2.18	67.39	87.13	4.00	58.18	82.51	2.15
CRT	52.31	81.14	1.98	68.38	88.13	1.48	62.46	83.50	1.79
CRT MULTI	53.00	81.99	2.31	69.01	90.01	1.23	64.40	84.54	1.94

classes, 500 samples per class and $10k$ validation images, with different simulated imbalances applied; (iii) *iNaturalist 2019* [60]: a challenging task for image classification in the wild comprised of $26k$ training and $3k$ validation images labeled with $1k$ classes, with skewed distribution in label frequency.

Imbalanced data learning. In Table 1 we compare the performance of CRT to other competing solutions, with each baseline carefully tuned to ensure fairness. In some cases we notice performance discrepancies compared to results reported by prior literature (in general our code runs better), which is explained in the SM. Overall, CRT-based solutions consistently lead the performance chart, with the label-prior variant solidly outperforming vanilla CRT and other competitors in most categories. While showing the varying degrees of success, FOCAL and LDAM failed to establish dominance comparing to ERM. GAN and VAT also verified the effectiveness of augmentation and adversarial perturbations in the imbalanced setting. In Figure 10 we also visualize the CRT learned representation using the tSNE embedding.

Learning efficiency. We further examine the dynamics of efficiency gains from CRT, with the results summarized in Figure 11. Consistent with the theoretical predictions based on the weak-supervision argument, increasing majority sample size improves the accuracy of minority identifications. Causal augmentation is especially effective in the low-sample regime, which offers more than $4\times$ boost in effective minority sample size. The performance gap between augmented and un-augmented solution

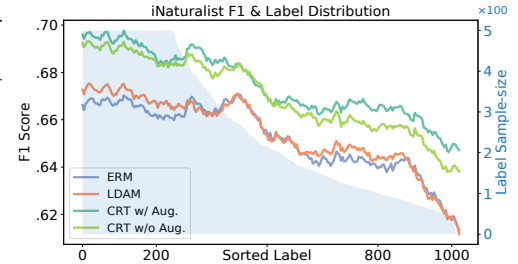


Figure 14. Class-conditional F1 curve for iNat2019.

closes as we increase minority sample, but it always improves. In Figure 12, we compare the same neural predictor trained respectively on the feature and source representations. Source modeling speeds up learning, in addition to the decent accuracy gains. Augmented training progresses a bit slower, but eventually converges to a better solution. In our experiments, the major performance boost comes from the GCL-based source space modeling we advocated, to a lesser extent from the augmentation perspective presented by [58]. Figure 14 gives the performance comparison of different learning schemes wrt different label sizes using the F1 score.

We also examined the contributions from augmentation as we vary the augmentation weight λ (Figure 13). We observe a relatively small λ already lends improvement, but a relatively large value degrades results when the minority size is small. This implies the augmentation gains are more likely to be originated from the exposure to the diversity of synthetic augments, and the accuracy of augmented distribution is limited by the imperfectness of empirical estimation (e.g., limited sample size).

6. Conclusion

This paper developed a novel learning scheme for imbalanced data learning. Leveraging a causal perspective, our solution cuts through the apparent data heterogeneities and identifies the shared invariant, disentangled source representation, using only majority samples. We demonstrate this source representation modeling enables more efficient learning and allows principled augmentation. In future work, we seek extended applications in non-vision settings.

References

- [1] A. Antoniou, A. Storkey, and H. Edwards. Data augmentation generative adversarial networks. *arXiv preprint arXiv:1711.04340*, 2017.
- [2] M. Arjovsky, L. Bottou, I. Gulrajani, and D. Lopez-Paz. Invariant risk minimization. *arXiv preprint arXiv:1907.02893*, 2019.
- [3] N. Bansal, X. Chen, and Z. Wang. Can we gain more from orthogonality regularizations in training deep networks? In *NIPS*, 2018.
- [4] Z. I. Botev and D. P. Kroese. An efficient algorithm for rare-event probability estimation, combinatorial optimization, and counting. *Methodology and Computing in Applied Probability*, 10(4):471–505, 2008.
- [5] P. Bühlmann. Invariance, causality and robustness. *arXiv preprint arXiv:1812.08233*, 2018.
- [6] J. Byrd and Z. Lipton. What is the effect of importance weighting in deep learning? In *ICML*, 2019.
- [7] K. Cao, C. Wei, A. Gaidon, N. Arechiga, and T. Ma. Learning imbalanced datasets with label-distribution-aware margin loss. In *NeurIPS*, 2019.
- [8] N. V. Chawla, K. W. Bowyer, L. O. Hall, and W. P. Kegelmeyer. SMOTE: synthetic minority over-sampling technique. *Journal of artificial intelligence research*, 16:321–357, 2002.
- [9] R. T. Chen, Y. Rubanova, J. Bettencourt, and D. K. Duvenaud. Neural ordinary differential equations. In *Advances in neural information processing systems*, pages 6571–6583, 2018.
- [10] A. Choromanska, A. Agarwal, and J. Langford. Extreme multi class classification. In *NIPS Workshop: eXtreme Classification, submitted*, volume 1, pages 2–1, 2013.
- [11] A. Chouldechova and A. Roth. The frontiers of fairness in machine learning. *arXiv preprint arXiv:1810.08810*, 2018.
- [12] M. Cogswell, F. Ahmed, R. Girshick, L. Zitnick, and D. Batra. Reducing overfitting in deep networks by decorrelating representations. *arXiv preprint arXiv:1511.06068*, 2015.
- [13] P. Comon. Independent component analysis, a new concept? *Signal processing*, 36(3):287–314, 1994.
- [14] C. Cortes and V. Vapnik. Support-vector networks. *Machine learning*, 20(3):273–297, 1995.
- [15] E. D. Cubuk, B. Zoph, D. Mane, V. Vasudevan, and Q. V. Le. Autoaugment: Learning augmentation strategies from data. In *CVPR*, 2019.
- [16] Y. Cui, M. Jia, T.-Y. Lin, Y. Song, and S. Belongie. Class-balanced loss based on effective number of samples. In *CVPR*, 2019.
- [17] A. Dal Pozzolo, G. Boracchi, O. Caelen, C. Alippi, and G. Bontempi. Credit card fraud detection: a realistic modeling and a novel learning strategy. *IEEE transactions on neural networks and learning systems*, 29(8):3784–3797, 2017.
- [18] G. Desjardins, K. Simonyan, R. Pascanu, et al. Natural neural networks. In *NIPS*, 2015.
- [19] T. A. Dingus, F. Guo, S. Lee, J. F. Antin, M. Perez, M. Buchanan-King, and J. Hankey. Driver crash risk factors and prevalence evaluation using naturalistic driving data. *Proceedings of the National Academy of Sciences*, 113(10):2636–2641, 2016.
- [20] C. Drummond, R. C. Holte, et al. C4. 5, class imbalance, and cost sensitivity: why under-sampling beats over-sampling. In *Workshop on learning from imbalanced datasets II*, volume 11, pages 1–8. Citeseer, 2003.
- [21] C. Elkan. The foundations of cost-sensitive learning. In *International joint conference on artificial intelligence*, volume 17, pages 973–978. Lawrence Erlbaum Associates Ltd, 2001.
- [22] L. Fei-Fei, R. Fergus, and P. Perona. One-shot learning of object categories. *IEEE transactions on pattern analysis and machine intelligence*, 28(4):594–611, 2006.
- [23] C. Finn, P. Abbeel, and S. Levine. Model-agnostic meta-learning for fast adaptation of deep networks. *arXiv preprint arXiv:1703.03400*, 2017.
- [24] Y. Freund and R. E. Schapire. A decision-theoretic generalization of on-line learning and an application to boosting. *Journal of computer and system sciences*, 55(1):119–139, 1997.
- [25] I. J. Goodfellow, J. Shlens, and C. Szegedy. Explaining and harnessing adversarial examples. *arXiv preprint arXiv:1412.6572*, 2014.
- [26] H. He, Y. Bai, E. A. Garcia, and S. Li. Adasyn: Adaptive synthetic sampling approach for imbalanced learning. In *2008 IEEE international joint conference on neural networks (IEEE world congress on computational intelligence)*, pages 1322–1328. IEEE, 2008.
- [27] C. Heinze-Deml, J. Peters, and N. Meinshausen. Invariant causal prediction for nonlinear models. *Journal of Causal Inference*, 6(2), 2018.
- [28] L. Huang, D. Yang, B. Lang, and J. Deng. Decorrelated batch normalization. In *CVPR*, 2018.
- [29] A. Hyvärinen and E. Oja. Independent component analysis: algorithms and applications. *Neural networks*, 13(4-5):411–430, 2000.
- [30] A. Hyvärinen and P. Pajunen. Nonlinear independent component analysis: Existence and uniqueness results. *Neural networks*, 12(3):429–439, 1999.

- [31] A. Hyvarinen, H. Sasaki, and R. Turner. Nonlinear ica using auxiliary variables and generalized contrastive learning. In *AISTATS*, pages 859–868, 2019.
- [32] K. Jia, S. Li, Y. Wen, T. Liu, and D. Tao. Orthogonal deep neural networks. *IEEE transactions on pattern analysis and machine intelligence*, 2019.
- [33] I. Kaggle. Planet: Understanding the amazon from space—kaggle. Consulté sur <https://www.kaggle.com/c/planet-understanding-the-amazon-from-space/data> (Consulté le: 2018-01-25), 2017.
- [34] A. Kessy, A. Lewin, and K. Strimmer. Optimal whitening and decorrelation. *The American Statistician*, 72(4):309–314, 2018.
- [35] I. Khemakhem, D. Kingma, R. Monti, and A. Hyvarinen. Variational autoencoders and nonlinear ICA: A unifying framework. In *AISTATS*, pages 2207–2217, 2020.
- [36] G. King and L. Zeng. Logistic regression in rare events data. *Political analysis*, 9(2):137–163, 2001.
- [37] S. Kotsiantis, D. Kanellopoulos, P. Pintelas, et al. Handling imbalanced datasets: A review. *GESTS International Transactions on Computer Science and Engineering*, 30(1):25–36, 2006.
- [38] B. Li, Y. Liu, and X. Wang. Gradient harmonized single-stage detector. In *AAAI*, 2019.
- [39] K.-C. Li. Sliced inverse regression for dimension reduction. *Journal of the American Statistical Association*, 86(414):316–327, 1991.
- [40] T.-Y. Lin, P. Goyal, R. Girshick, K. He, and P. Dollár. Focal loss for dense object detection. In *Proceedings of the IEEE international conference on computer vision*, pages 2980–2988, 2017.
- [41] Z. Liu, Z. Miao, X. Zhan, J. Wang, B. Gong, and S. X. Yu. Large-scale long-tailed recognition in an open world. In *CVPR*, 2019.
- [42] J. T. Machado and A. M. Lopes. Rare and extreme events: the case of covid-19 pandemic. *Nonlinear Dynamics*, page 1, 2020.
- [43] G. Mariani, F. Scheidegger, R. Istrate, C. Bekas, and C. Malossi. BAGAN: Data augmentation with balancing GAN. *arXiv preprint arXiv:1803.09655*, 2018.
- [44] T. Miyato, S.-i. Maeda, M. Koyama, and S. Ishii. Virtual adversarial training: a regularization method for supervised and semi-supervised learning. *IEEE transactions on pattern analysis and machine intelligence*, 41(8):1979–1993, 2018.
- [45] M. M. Moya and D. R. Hush. Network constraints and multi-objective optimization for one-class classification. *Neural networks*, 9(3):463–474, 1996.
- [46] S. S. Mullick, S. Datta, and S. Das. Generative adversarial minority oversampling. In *ICCV*, pages 1695–1704, 2019.
- [47] G. Papamakarios, T. Pavlakou, and I. Murray. Masked autoregressive flow for density estimation. In *NIPS*, 2017.
- [48] J. Peters, P. Bühlmann, and N. Meinshausen. Causal inference using invariant prediction: identification and confidence intervals. *Journal of the Royal Statistical Society Series B (Statistical Methodology)*, 2016.
- [49] D. J. Rezende and S. Mohamed. Variational inference with normalizing flows. *arXiv preprint arXiv:1505.05770*, 2015.
- [50] J. Robinson, S. Jegelka, and S. Sra. Strength from weakness: Fast learning using weak supervision. In *ICML*, 2020.
- [51] M. Rojas-Carulla, B. Schölkopf, R. Turner, and J. Peters. Invariant models for causal transfer learning. *The Journal of Machine Learning Research*, 19(1):1309–1342, 2018.
- [52] D. Rothenhäusler, N. Meinshausen, P. Bühlmann, and J. Peters. Anchor regression: heterogeneous data meets causality. *arXiv preprint arXiv:1801.06229*, 2018.
- [53] L. Ruff, R. Vandermeulen, N. Goernitz, L. Deecke, S. A. Siddiqui, A. Binder, E. Müller, and M. Kloft. Deep one-class classification. In *ICML*, 2018.
- [54] B. Schölkopf, D. Janzing, J. Peters, E. Sgouritsa, K. Zhang, and J. Mooij. On causal and anticausal learning. *arXiv preprint arXiv:1206.6471*, 2012.
- [55] C. Shorten and T. M. Khoshgoftaar. A survey on image data augmentation for deep learning. *Journal of Big Data*, 6(1):60, 2019.
- [56] N. Siddharth, B. Paige, J.-W. Van de Meent, A. Desmaison, N. Goodman, P. Kohli, F. Wood, and P. Torr. Learning disentangled representations with semi-supervised deep generative models. In *NIPS*, 2017.
- [57] C. Szegedy, V. Vanhoucke, S. Ioffe, J. Shlens, and Z. Wojna. Rethinking the inception architecture for computer vision. In *CVPR*, 2016.
- [58] T. Teshima, I. Sato, and M. Sugiyama. Few-shot domain adaptation by causal mechanism transfer. 2020.
- [59] P. Tokmakov, Y.-X. Wang, and M. Hebert. Learning compositional representations for few-shot recognition. In *Proceedings of the IEEE International Conference on Computer Vision*, pages 6372–6381, 2019.
- [60] G. Van Horn, O. Mac Aodha, Y. Song, Y. Cui, C. Sun, A. Shepard, H. Adam, P. Perona, and S. Belongie. The iNaturalist species classification and detection dataset. In *Proceedings of the IEEE conference on computer vision and pattern recognition*, pages 8769–8778, 2018.
- [61] V. Vapnik. *The nature of statistical learning theory*. Springer science & business media, 2013.

- [62] O. Vinyals, C. Blundell, T. Lillicrap, D. Wierstra, et al. Matching networks for one shot learning. In *NIPS*, 2016.
- [63] Y. Wang, Q. Yao, J. T. Kwok, and L. M. Ni. Generalizing from a few examples: A survey on few-shot learning. *ACM Computing Surveys (CSUR)*, 53(3):1–34, 2020.
- [64] Y.-X. Wang, D. Ramanan, and M. Hebert. Learning to model the tail. In *NIPS*, 2017.
- [65] J. Wu, Q. Zhang, and G. Xu. Tiny imagenet visual recognition challenge. <https://www.kaggle.com/c/tiny-imagenet>, 2017. [Online; accessed 2020-11-10].

Supercharging Imbalanced Data Learning With Causal Representation Transfer (Supplementary Material)

A. Theoretical Support

Here we summarize some theories from literature that supports the development of this paper by making it self-contained. Attempts have been made to unify the notations, making them consistent with our paper, and also drop some contents from the original presentations that not directly relevant in this context.

A.1. Nonlinear ICA with auxiliary variables

The following theory lists the technical conditions required for the identification of conditional nonlinear ICA model, based on which our work was built.

Definition A.1 (Conditionally exponential of order k). A random variable (independent component) $[s]_i$ is conditionally exponential of order k given random vector \mathbf{c} if its conditional pdf can be given in the form

$$p([s]_i|\mathbf{c}) = \frac{Q_i([s]_i)}{Z_i(\mathbf{c})} \exp \left[\sum_{j=1}^k \tilde{q}_{ij}([s]_i) \lambda_{ij}(\mathbf{c}) \right] \quad (6)$$

almost everywhere in the support of \mathbf{c} , with $\tilde{q}_{ij}, \lambda_{ij}, Q_i$ and Z_i scalar-valued functions. The sufficient statistics \tilde{q}_{ij} are assumed linearly independent.

Theorem A.2 (Theorem 3, [31], identification of Nonlinear ICA). Assume (i) the data follows the nonlinear ICA model with the conditional independence $q(\mathbf{s}|\mathbf{c}) = \prod_j q_j([s]_j|\mathbf{c})$; (ii) Each $[s]_j$ is conditionally exponential given \mathbf{c} (Definition A.1); (iii) There exist $nk + 1$ points $\mathbf{c}_0, \dots, \mathbf{c}_{nk}$, such that the following matrix of size $nk \times nk$

$$\tilde{\mathbf{L}} = \begin{pmatrix} \lambda_{11}(\mathbf{c}_1) - \lambda_{11}(\mathbf{c}_0) & \cdots & \lambda_{11}(\mathbf{c}_{nk}) - \lambda_{11}(\mathbf{c}_0) \\ \lambda_{nk}(\mathbf{c}_1) - \lambda_{nk}(\mathbf{c}_0) & \cdots & \lambda_{nk}(\mathbf{c}_{nk}) - \lambda_{nk}(\mathbf{c}_0) \end{pmatrix} \quad (7)$$

is invertible; (iv) nonlinear Logistic regression system Eqn (1) is trained using functions with universal approximation capacity. Then in the limit of infinite data, $f(\mathbf{z})$ provides a consistent estimator of the nonlinear ICA model, up to a linear transformation of point-wise scalar functions of the independent components.

A.2. Variance and generalization bound

The following theories explore the consequence of training using only nonparametric causal augmentation. First we define the risk estimators.

Definition A.3. Let \tilde{S} be the non-parametric source augmentation defined in Eqn (3) main text, $\ell(\cdot)$ be the loss function, $g(\mathbf{z})$ be the hypothesis function. We define the risk R and causally augmented risk estimator \tilde{R} wrt g respectively as

$$R(g) \triangleq \mathbb{E}_Z[\ell(g(Z))], \tilde{R}(g) \triangleq \mathbb{E}_{\tilde{S}}[\ell(g(\hat{f}^{-1}(\tilde{S})))] \quad (8)$$

where \hat{f} is the estimated causal de-mixing function.

The following theorem revealed that assuming perfect knowledge of de-mixing function f , the causally augmented risk estimator is optimal.

Theorem A.4 (Theorem 1, [58], minimum variance property). Assuming $\hat{f} = f$. Then for each $g \in \mathcal{G}$, the causal augmented risk estimator $\tilde{R}(g)$ is the uniformly minimum variance unbiased estimator of $R(g)$, i.e., $\mathbb{E}[\tilde{R}(g)] = R(g)$ and for any unbiased estimator \tilde{R} of $R(g)$ (i.e., $\mathbb{E}[\tilde{R}(g)] = R(g)$),

$$\text{Var}[\tilde{R}(g)] \leq \text{Var}[\tilde{R}(g)]. \quad (9)$$

Since we are bound to have estimation errors, the next theorem establishes the generalization bounds wrt such errors.

Theorem A.5 (Theorem 2, [58], excess risk bound). *Let $\check{g} = \arg \min \check{R}$ and $g^* = \arg \min R(g)$, then under appropriate assumptions (Assumptionss 1-8 in [58]), for arbitrary $\delta, \delta' \in (0, 1)$, we have probability at least $1 - (\delta + \delta')$,*

$$R(\check{g}) - R(g^*) \leq \underbrace{C \sum_{j=1}^d \|f_j - \hat{f}\|_{W^{1,1}}}_{\text{Approximation error}} + \underbrace{4d\mathfrak{R}(\mathcal{G}) + 2dB_\ell \sqrt{\frac{\log 2/\delta}{2n}}}_{\text{Estimation error}} + \underbrace{\kappa_1(\delta', n) + dB_\ell B_q \kappa_2(f - \hat{f})}_{\text{Higher-order terms}}. \quad (10)$$

Here $\|\cdot\|_{W^{1,1}}$ is the Sobolev norm and $\mathfrak{R}(\mathcal{G})$ is the effective Rademacher complexity defined by

$$\mathfrak{R}(\mathcal{G}) \triangleq \frac{1}{n} \mathbb{E}_{\hat{\mathcal{S}}} \mathbb{E}_{\sigma} \left[\sup_{g \in \mathcal{G}} \left| \sum_{i=1}^n \sigma_i s \mathbb{E}_{S'_2, \dots, S'_d} \tilde{\ell}(\hat{s}_i, S'_2, \dots, S'_d) \right| \right], \quad (11)$$

where $\{\sigma_i\}_{i=1}^n$ are independent sign variables, $\mathbb{E}_{\hat{\mathcal{S}}}$ is the expectation wrt $\{\hat{s}_i\}_{i=1}^n$, the dummy variables S'_2, \dots, S'_d are i.i.d. copies of \hat{s}_1 , and $\tilde{\ell}$ is defined by

$$\tilde{\ell}(s_1, \dots, s_d) \triangleq \frac{1}{d!} \sum_{\pi} \ell(g, \hat{f}^{-1}(s_{\pi(1)}, \dots, s_{\pi(d)})), \quad (12)$$

where π denotes the permutations. κ_1, κ_2 are higher order terms, B_q, B_ℓ respectively depends on density q and loss ℓ , while C' depends on (f, q, ℓ, d) .

A.3. Speedup from weak supervision

[50] built some interesting theories trying to answer the following question: “Can large amounts of weakly labeled data provably help learn a better model than strong labels alone?” We summarize its main findings below and elaborate how it lends support for CRT.

In the setting of weakly supervised learning, we have the triplet $(\mathcal{X}, \mathcal{W}, \mathcal{Y})$, where \mathcal{X} and \mathcal{Y} respectively denote the features and labels of interest (strong task), and \mathcal{W} denote weak task labels that are relevant to the prediction of \mathcal{Y} . It is assumed that there is this unknown good embedding $Z = f_0(X)$ that predicts W , that could be leveraged to derive a model of the form $\hat{g}(\cdot, \hat{f}) : \mathcal{X} \rightarrow \mathcal{Y}$ that improves learning.

Algorithm 2 Weakly supervised learning

1. Pretrain encoder with weak labels

$$\hat{f} \leftarrow \text{Alg}(\mathcal{F}, \mathbb{P}_{XW})$$

2. Augment data with

$$z_i = \hat{f}(x_i) \Rightarrow \{(x_i, y_i, z_i)\} \sim \hat{\mathbb{P}}_{XYZ}$$

3. Optimize the strong task

$$\hat{g} \leftarrow \text{Alg}(\mathcal{G}, \hat{\mathbb{P}}_{XYZ})$$

Theorem A.6 (Theorem 3, [50]). *Suppose that $\text{Rate}_m(\mathcal{F}, \mathbb{P}_{XW}) = \mathcal{O}(m^{-\alpha})$ and that $\text{Alg}_n(\mathcal{G}, \hat{\mathbb{P}})$ is ERM. Under suitable assumptions on $(\ell, \mathbb{P}, \mathcal{F})$, Algorithm 2 obtains excess risk*

$$\mathcal{O}\left(\frac{\alpha\beta \log n + \log(1/\delta)}{n} + \frac{1}{n^{\alpha\beta}}\right) \quad (13)$$

with probability $1 - \delta$, when $m = \Omega(n^\beta)$ for \mathcal{W} discrete, or $m = \Omega(n^{2\beta})$ for \mathcal{W} continuous.

For concrete examples, in a typical learning scenario where $\text{Alg}_m(\mathcal{F}, \mathbb{P}_{XW}) = \mathcal{O}(m^{-1/2})$, one obtains the fast rates $\mathcal{O}(1/n)$ for $m = \Omega(n^2)$.

In the context of our CRT, we identify the learning of common causal de-mixing function $f(z)$ as the weak learning task, and the source space \mathcal{S} is the common embedding space of interest, that can be leveraged to improve the learning of the main classification task.

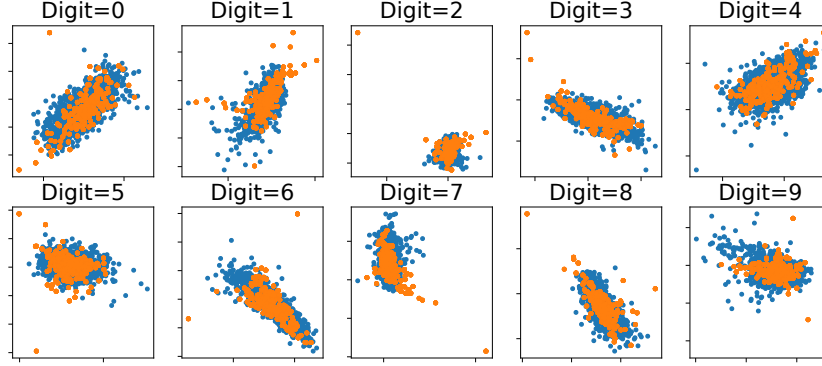


Figure S1. Feature space augmentation for MNIST.

B. Regression for continuous labels

We can further extend the applicability of the proposed CRT to the case of regressing continuous outcomes. While in principle, the procedures described in Sec 3 can be readily applied, we advocate coarse graining wrt label y similar to what has been practiced in *sliced inverse regression* [39], especially when the feature dimension is high relative to the sample size. Specifically, we partition y into different bins, and use feed the bin label as the conditioning variable in the GCL step. We still use the regression loss for the training of encoder and predictors.

C. Implementation of Augmentation

Let $\hat{s}_i^k, i = 1, \dots, n_k$ be the estimated source representation for the k -th class.

- Non-parametric augmentation: shuffling indices as described in the main text.
- Parametric augmentation: estimate $\hat{\mu}_k = \text{mean}(\hat{s}^k), \hat{\sigma}_k = \text{std}(\hat{s}^k)$, then $s^{k, \text{aug}} \sim \mathcal{N}(\hat{\mu}_k, \hat{\sigma}_k^2)$.
- Oracle augmentation: nonparametric augmentation with an abundance of class-conditional source space samples .

In Figure 9 from main text we compare the efficiency of parametric and nonparametric augmentation schemes under different minority sample size. In particular, we compute the MMD distance $\|\hat{\mu}_{\text{aug}} - \hat{\mu}_{\text{ref}}\|_\kappa$, where $\hat{\mu}_{\text{aug}} = \sum_i \kappa(\tilde{s}_i, \cdot)$ and $\hat{\mu}_{\text{ref}} = \sum_i \kappa(s_i, \cdot)$. Here $\kappa(\cdot, \cdot)$ is the Gaussian rbf kernel $\kappa(x, y) = \exp(\|x - y\|^2 / 2\sigma^2)$, $\|f\|_\kappa = \sqrt{\langle f, f \rangle_\kappa}$ is the RKHS norm and \tilde{s}_i, s_i respectively denote augmented class-conditional samples (from few minority samples) and empirical distribution of class-conditional samples (where we use all samples from the same class that we holdout). In this example we use $2k$ samples for the ground truth and augment minority to the same size. Different kernel bandwidth σ of κ yields qualitatively similar results, and in the paper we report the one with $\sigma = 0.5$.

In Figure S1, we visualize the augmentation in feature space for the MNIST dataset. And we see for boundary points the discrepancy can be amplified by the neural network inversion, which partly explained the sub-optimal performance from feature space augmentation. In contrast, the source space augmentation advocated in this paper is more computationally efficient and robust.

Note that while in principle the majority classes can be similarly augmented, we choose not to refine our model with the augmented majorities. This decision is justified by the classical consideration for bias-variance trade-off: estimation errors of $f(z)$ is inevitable (e.g., finite sample size, SGD, limited network capacity, etc.), and they will carry over to the augmented samples, resulting biases in the augmented estimation of our predictor. On the other hand, using augmented samples helps bring down estimation variance. For minority labels, the reduction in variance is greater than the induced bias, and consequently merits the application of CRT to improve performance. For majority labels, this might not be the case.

D. Toy Model Experiment

D.1. Toy Data Illustration

We sample seven groups of two-dimensional uncorrelated Gaussian of each with size 2000, with different means and variances as our real source representation s . Specifically, $s_i \sim N(\mu_i, \Sigma_i), i = 0, \dots, 6$, where $\mu_0 = [-0.5, -1], \mu_1 =$

$[2, 1], \mu_2 = [5, 2], \mu_3 = [1, 3], \mu_4 = [-2, 1], \mu_5 = [-3.5, 4], \mu_6 = [-4, -1], \Sigma_0 = [0.5, 0.5], \Sigma_1 = [3, 1], \Sigma_2 = [1, 2], \Sigma_3 = [0.3, 2], \Sigma_4 = [1, 0.2], \Sigma_5 = [1, 1], \Sigma_6 = [2, 0.3]$. Then we perform classical Hénon transformation $z_{(1)} = 1 - 1.4 \tilde{s}_{(1)}^2 + \tilde{s}_{(2)}, z_{(2)} = 0.3, \tilde{s}_{(1)}$ to generate the data in feature space.

D.2. Extreme-classification Toy Data

We sample 1000 groups of two-dimensional uncorrelated Gaussian with mean ranges uniformly sampled from range $(-4, 4)$ and standard deviation fixed to 0.1. Validation dataset is fixed with 20 samples per-class, and the sampler per class in training dataset varies with 5, 10, 20, 50, 75, 100, 150. The summary for extreme-classification is presented in Table S1.

Note that when the total number of categories is 10 with 20 samples per class, ERM has top-1 accuracy as high as 0.914, and the performance drops when the number of categories increasing. With 500 categories, the accuracy decreases to 0.005, and in the scenario where we presented in the main text with 1000 categories, ERM performs no better than random guessing.

Table S1. Validation Results for Extreme classification

Metric	NLL			Top 1			Top5		
SAMPLE-SIZE	ERM	CRT W/O AUG	CRT	ERM	CRT W/O AUG	CRT	ERM	CRT W/O AUG	CRT
5	6.9246	4.3884	3.7098	0.0015	0.0450	0.0760	0.0053	0.2275	0.3220
10	6.9242	4.0536	3.4752	0.0018	0.0638	0.0856	0.0060	0.2666	0.3549
20	6.9185	3.5405	3.3657	0.0016	0.0741	0.0877	0.0070	0.3126	0.3675
50	6.9240	3.3794	3.2957	0.0010	0.0834	0.0934	0.0045	0.3493	0.3835
75	6.9190	3.3499	3.2594	0.0020	0.0846	0.0939	0.0060	0.3571	0.3950
100	6.9182	3.3394	3.2675	0.0020	0.0834	0.0934	0.0053	0.3580	0.3918
150	6.9174	3.2731	3.2597	0.0011	0.0906	0.0984	0.0059	0.3777	0.4034

E. Image Data Experiments

We summarized the image datasets in Table S2 and the network architectures used for respective datasets in Tables S3, S4, S5 and S6. The hyperparameters we used in these experiments are presented in S9. The results reported here are from our regularized non-parametric CRT implementation, parametric CRT implementation show a similar trend, with slightly improved performance (results now shown). We use 2 latent dims for MNIST and 32 latent dims for CIFAR100, iNaturalist and Tiny-Imagenet.

Preprocessing For iNaturalist dataset, we used pretrained Inception V3 to extract the features with dim=2048. For Tiny-Imagenet we finetuned the Resnet 18 to extract the features with dim = 512.

Baselines We used the ERM, LDAM (<https://github.com/kaidic/LDAM-DRW>), Focal (<https://github.com/artemavrin/focal-loss>), IW (<https://github.com/idiap/importance-sampling>), and VAT implementation from <https://github.com/lyakaap/VAT-pytorch>. For GAN we adopted the CGAN model with architecture shown in S8 and noise dimension listed in S10 for each dataset. We compared all the models with their own best performance after early stopping.

Discrepancy of baseline performance. We noticed that our implementation of baseline models, especially for the ERM baseline, yields results better than what's reported in literature (LDAM in particular). Specifically, our results look better. After carefully compared our implementation to the LDAM codebase, we see that the discrepancy comes from the choice of optimizer. The use of vanilla SGD optimizer, as practiced in LDAM, results in degraded performance of baseline, and consequently a larger performance gap compared to strong solutions.

Majority bias. In Figure S3, we give the top-1 accuracy wrt different minority size on the iNaturalist dataset. This figure is complementary to the F1-label frequency plot given in Figure 14 from the main text. While the improvement at the tail part are strong under both metrics, we see clear evidence of majority bias in the Top-1 accuracy plot. ERM and LDAM show better performance in accuracy for the sample abundant majority regime, but severe performance drop in the sample deficient minority regime. This is because ERM and alike finds it more rewarding to favor the majorities during inference, which gives better sensitivity but much worse specificity for the majority samples, and consistently hurting the performance for minorities.

Table S2. Summary of datasets

NAME	DIM	TRAIN (MAJORITY)	TRAIN (MINORITY)	VALIDATION
MNIST	(28×28)	$6000 \times (1 \text{ OR } 5) \text{ (CLS)}$	$1200 \times (1 \text{ OR } 5) \text{ (CLS)}$	$1000 \times 10 \text{ (CLS)}$
CIFAR	$(32 \times 32 \times 3)$	$500 \times 50 \text{ (CLS)}$	$500 \times 50 \text{ (CLS)}$	$100 \times 100 \text{ (CLS)}$
INAT	$(\text{NONE} \times \text{NONE} \times 3)$	$(\geq 120) \times 725 \text{ (CLS)}$	$(< 120) \times 285 \text{ (CLS)}$	$3 \times 1010 \text{ (CLS)}$
TINY	$(64 \times 64 \times 3)$	$450 \times 100 \text{ (CLS)}$	$45 \times 100 \text{ (CLS)}$	$50 \times 200 \text{ (CLS)}$

Table S3. MNIST experiment network architecture.

NETWORK	ARCHITECTURE
ENCODER	FC(UNIT=32)+RELU + FC(UNIT=32)+RELU + FC(UNIT=2)
DECODER	FC(UNIT=32)+RELU + FC(UNIT=32)+RELU + FC(UNIT=10)
FLOW	MAF($n_{blocks} = 4$, $hidden_{size} = 128$, $n_{hidden} = 2$).

Table S4. Cifar100 experiment network architecture.

NETWORK	ARCHITECTURE
ENCODER	RESNET18 ^a + FC(UNIT=32)
DECODER	FC(UNIT=256)+RELU FC(UNIT=100)
FLOW	MAF($n_{blocks} = 4$, $hidden_{size} = 128$, $n_{hidden} = 2$).

^aResnet 18 without last layer

TABLE S5. INATURALIST EXPERIMENT NETWORK ARCHITECTURE.

NETWORK	ARCHITECTURE
PRETRAIN	INCEPTION(V3)
ENCODER	FC(UNIT=1024)+RELU +DROPOUT(0.1) + FC(UNIT=512)+RELU +DROPOUT(0.1) + FC(UNIT=32)
DECODER	FC(UNIT=32)+RELU +DROPOUT(0.1) + FC(UNIT=512)+RELU +DROPOUT(0.1) + FC(UNIT=1010)
FLOW	MAF($n_{blocks} = 4$, $hidden_{size} = 128$, $n_{hidden} = 2$).

TABLE S6. TINY IMAGENET EXPERIMENT NETWORK ARCHITECTURE.

NETWORK	ARCHITECTURE
PRETRAIN	RESNET18
ENCODER	FC(UNIT=1024)+RELU +DROPOUT(0.1) + FC(UNIT=512)+RELU +DROPOUT(0.1) + FC(UNIT=32)
DECODER	FC(UNIT=512)+RELU +DROPOUT(0.1) + FC(UNIT=200)
FLOW	MAF($n_{blocks} = 4$, $hidden_{size} = 128$, $n_{hidden} = 2$).

Table S7. MNIST results with different numbers of minority categories

# MINORITY LABEL	1		5	
	NLL	TOP 1	NLL	TOP 1
ERM	0.342	0.933	0.390	0.904
LDAM	1.6737	0.9609	1.50	0.940
CRT	0.186	0.972	0.257	0.950

TABLE S8. GAN NETWORK ARCHITECTURE.	
NETWORK	ARCHITECTURE
GENERATOR	FC(UNIT=256) +LEAKYRELU + FC(UNIT=256)+LEAKYRELU +FC(UNIT=LATENT _{dim})
DISCRIMINATOR	FC(UNIT=256) +LEAKYRELU +DROPOUT(0.1) + FC(UNIT=256)+LEAKYRELU +DROPOUT(0.1) +FC(UNIT=1)+SIGMOID

TABLE S9. HYPERPARAMETER OF DATASETS (CRT)

NAME	REG WEIGHT	AUG STRENGTH
MNIST	1E-2	1E-3
CIFAR	1E-2	1E-3
INAT	5E-3	1E-3
TINY	1E-3	1E-3

TABLE S10. HYPERPARAMETER OF DATASETS (GAN)

NAME	NOISE DIM
MNIST	32
CIFAR	64
INAT	128
TINY	128

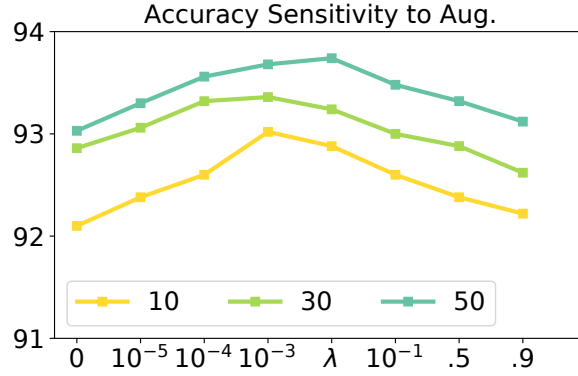


Figure S2. Sensitivity analysis (overall top 1 accuracy) of augmentation strength λ . (Complementing Figure 13.)

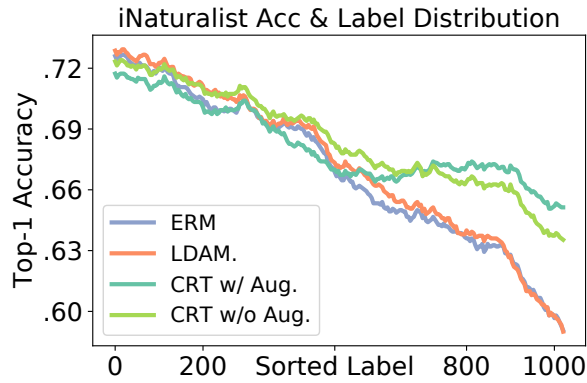


Figure S3. Class-conditional Top-1 accuracy curve for iNat2019.